General Disclaimer

One or more of the Following Statements may affect this Document

- This document has been reproduced from the best copy furnished by the organizational source. It is being released in the interest of making available as much information as possible.

- This document may contain data, which exceeds the sheet parameters. It was furnished in this condition by the organizational source and is the best copy available.

- This document may contain tone-on-tone or color graphs, charts and/or pictures, which have been reproduced in black and white.

- This document is paginated as submitted by the original source.

- Portions of this document are not fully legible due to the historical nature of some of the material. However, it is the best reproduction available from the original submission.

OLD DOMINION UNIVERSITY RESEARCH FOUNDATION

DEPARTMENT OF PHYSICS AND GEOPHYSICAL SCIENCES
SCHOOL OF SCIENCES AND HEALTH PROFESSIONS
OLD DOMINION UNIVERSITY
NORFOLK, VIRGINIA

Technical Report PGSTR-AP78-9

AN EXPERIMENTAL/ANALYTICAL PROGRAM TO ASSESS THE UTILITY OF LIDAR FOR POLLUTION MONITORING

By

Frank S. Mills

Robert J. Allen

Carolyn F. Butler

Earl C. Kindle, Principal Investigator

Final Report
For the period September 1, 1976 - October 31, 1977

Prepared for the
National Aeronautics and Space Administration
Langley Research Center
Hampton, Virginia 23665

Under
Research Grant NSG 1343
E. V. Browell, Technical Monitor
Atmospheric Environmental Sciences Division

June 1978

DEPARTMENT OF PHYSICS AND GEOPHYSICAL SCIENCES
SCHOOL OF SCIENCES AND HEALTH PROFESSIONS
OLD DOMINION UNIVERSITY
NORFOLK, VIRGINIA

Technical Report PGSTR-AP78-9

AN EXPERIMENTAL/ANALYTICAL PROGRAM TO ASSESS THE UTILITY OF LIDAR FOR POLLUTION MONITORING

By

Frank S. Mills

Robert J. Allen

Carolyn F. Butler

Earl C. Kindle, Principal Investigator

Final Report
For the period September 1, 1976 - October 31, 1977

Prepared for the
National Aeronautics and Space Administration
Langley Research Center
Hampton, Virginia 23665

Under
Research Grant NSG 1343
E. V. Browell, Technical Monitor
Atmospheric Environmental Sciences Division

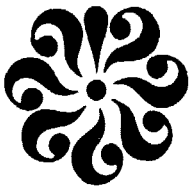

Submitted by the
Old Dominion University Research Foundation
P.O. Box 6369
Norfolk, Virginia 23508

June 1978

TABLE OF CONTENTS

LIST OF TABLES

LIST OF FIGURES

AN EXPERIMENTAL/ANALYTICAL PROGRAM TO ASSESS THE UTILITY OF LIDAR FOR POLLUTION MONITORING

By

Frank S. Mills[1], Robert J. Allen[2], and Carolyn F. Butler[2]

1. INTRODUCTION

The aim of the research performed under this grant was the development and demonstration of lidar techniques for the remote measurement of atmospheric constituents and transport processes in the lower troposphere. Particular emphasis was given to techniques for monitoring SO_2 and particulates, the principal pollutants in power plant and industrial plumes. Data from a plume dispersion study conducted in Maryland during September and October 1976 were reduced, and a data base was assembled which is available to the scientific community for plume model verification. (The mobile ruby lidar system used in the study was constructed under a previous grant, reference 1). A UV Differential Absorption Lidar (DIAL) was built, and preliminary testing was done. Work on the development of an IR DIAL system proceeded.

This report will describe in detail the accomplishments in all areas mentioned above. Section 2 describes a study of the effect of transient digitizer errors on DIAL measurements conducted by Frank S. Mills of Old Dominion University and Edward V. Browell of NASA Langley Research Center. A paper describing this study was presented at the Eighth International Laser Radar Conference in June 1977 (ref. 2). This study is pertinent to all DIAL systems including the UV and IR DIAL systems.

Section 3 contains a description of the UV DIAL system. The system was designed and constructed by Robert J. Allen and Lawrence Perillo of Old Dominion University working with NASA LaRC personnel using a double-

[1] Research Assistant Professor of Physics and Geophysical Sciences, Old Dominion University, Norfolk, Virginia 23508.

[2] Graduate Research Assistant, Department of Physics and Geophysical Sciences, Old Dominion University, Norfolk, Virginia 23508.

pulse laser concept developed by Dr. Browell at NASA LaRC. Dr. Mills was responsible for data acquisition system hardware and software for the UV DIAL. A paper describing the UV DIAL system was presented at the Eighth International Laser Radar Conference in June 1977 (ref. 3).

Section 4 briefly describes progress made on the IR DIAL system. Progress was limited since the laser delivery was delayed due to problems encountered by the laser manufacturer. Much of the data acquisition system software developed for the UV DIAL system will also be applicable to the IR DIAL system.

Section 5 is a report of the plume dispersion study which was conducted during September and October 1976 including a description of the mobile lidar system, the experimental design, the data reduction process, and the resulting data base. This study was sponsored on a cooperative basis by NASA and the State of Maryland Power Plant Siting Program with participation by a number of other organizations including Old Dominion University, Wyle Laboratories, Martin Marietta Research Laboratories, Environmental Measurements Incorporated, Engineering-Test Services, and the Potomac Electric Power Company. Old Dominion University personnel involved in the study were Dr. Mills and Carolyn F. Butler. A paper describing the study was presented at the Eighth International Laser Radar Conference in June 1977 (ref. 4).

During the grant period, Ms. Butler completed a two-dimensional modeling study of the stratospheric transport of volcanic aerosols. This work has been reported elsewhere (refs. 5, 6).

Also during the grant period, Neale Mayo, a graduate research assistant in the Department of Physics and Geophysical Sciences at Old Dominion University, worked on the development of lidar systems at NASA LaRC. Much of his work is reported here.

2. THE EFFECT OF TRANSIENT DIGITIZER ERRORS ON DIAL MEASUREMENTS

This study was prompted by errors encountered in analyzing atmospheric returns from the near-IR DIAL system at NASA Langley Research Center which is used to measure vertical water vapor profiles. Figure 1 shows an example of the problem encountered. An exponentially decaying test signal was fed

through both channels of the data system, and a concentration profile was calculated in exactly the same way as for atmospheric returns. The large excursions at 1.0 and 2.0 km are caused by amplifier switching transients. The anomalies at 0.35 and 1.5 km are the ones which motivated this study.

In order to understand these anomalies it is necessary to describe how the concentration is calculated, and then to describe how the transient digitizer operates.

The DIAL concept is described in detail in section 3. Therefore only those aspects pertaining to this study will be discussed here.

The average concentration of the gas of interest in the range between ranges R_1 and R_2 is given by

$$NA = \frac{1}{2(R_2 - R_1)\left[\sigma_A(\lambda_{on}) - \sigma_A(\lambda_{off})\right]} \ln\left[\frac{P_{r,on}(R_1) \times P_{r,off}(R_2)}{P_{r,off}(R_1) \times P_{r,on}(R_2)}\right] \quad (1)$$

where $\sigma_A(\lambda_{on}) - \sigma_A(\lambda_{off})$ is the difference in the absorption cross section of the gas of interest at the on and off wavelengths; $P_{r,on}(R_i)$ is the power received at the wavelength from range R_i; and $P_{r,off}(R_i)$ is the power received at the off wavelength from range R_i. Before the concentration is calculated, the received signals are usually smoothed by performing a running average. The averaging interval is typically the same as the range cell length $R_2 - R_1$, although a smaller interval could just as easily be used.

One of the transient digitizers studied was the Biomation model 8100. This unit is capable of sampling an analog input at sample intervals as short as 10 ns, converting the analog samples to digital form, and storing the samples in a 2048-word memory. The digital resolution of the unit is 8 bits or 1 part in 256. For sample intervals as short as 100 ns the unit has the additional capability of accepting 2 independent analog inputs, which are designated channel A and channel B. In this mode of operation the analog inputs are sampled alternately, and the wave forms are stored in memory so that the even-numbered points contain the digital equivalent of the channel A input and the odd-numbered points contain the digital equivalent of the channel B input. For each channel the input signal is fed

through an input attenuator and a fixed gain video amplifier. The output of the video amplifier is then fed through a folding amplifier or full wave rectifying amplifier and then to the analog to digital converter. The folding amplifier passes positive signals unchanged and inverts negative signals. A sign bit is generated if the input was initially negative and inverted by the folding amplifier. Thus the folding amplifier produces the most significant or "sign" bit of the analog to digital conversion and reduces the dynamic range requirement for the remainder of the conversion by a factor of two. The remaining seven bits of analog to digital conversion are produced by a parallel comparator type of converter.

The primary difficulty encountered with this type of transient digitizer is a discontinuity in the digitized wave form at the point where the input signal crosses zero. This is the source of the anomalies shown in figure 1. There is an adjustment in the digitizer, the crossover adjustment, which can be set to eliminate the discontinuity, but the adjustment is very delicate and temperature sensitive, particularly when the unit is operating in the two-channel mode. Three different Biomation 8100 digitizers were investigated, and they all exhibited the same behavior, which indicates that the problem is inherent in the design and not just a peculiarity associated with one unit.

Figure 2 shows schematically how the calculated concentration is affected by the two different types of crossover misadjustment. It should be pointed out that if the discontinuity is of the same kind and magnitude and occurs at the same point in time for both the on and off wavelength return, there will be no anomaly in the calculated concentration, since the ratio of received powers in the argument of the logarithm in equation (1) remains unchanged.

A number of tests were performed on the Biomation 8100 using a decaying exponential signal as the input to simulate lidar returns. In the first series of tests, the same signal was fed to both channel A and channel B. The crossover adjustment for each channel was carefully adjusted to eliminate the discontinuity at the zero crossing point. This was verified by observing the digitized wave form for each channel as reproduced by the computer. One hundred wave forms on each channel were averaged and the concentration calculated assuming that a water vapor measurement was being made. For this test the calculated concentration showed no anomaly at the zero

crossing point. The second test used the same data except that the channel A data was shifted with respect to channel B by an amount which would be equivalent to 390 m before the concentration calculation was made. In this case, since the zero crossings occur at different times, the anomaly associated with the crossover misadjustment appeared even though every effort was made to adjust the crossover properly.

It was observed while making the crossover adjustment that the adjustment appeared to be most unstable and sensitive when the positive and negative parts of the wave form were correctly matched. It was therefore decided to adjust the crossover for each channel so that there was a small gap in the digitized wave form similar to the left-hand side of figure 2 and correct for the misadjustment analytically. First a slowly decaying signal was fed to each channel, and the average size of the gap was measured for each channel for 100 input wave forms. Next the first test was repeated, and the gap previously measured for each channel was subtracted from the portion of each input wave form which was greater than zero. As before, 100 wave forms on each channel were averaged and the concentration calculated with channel A shifted 390 m with respect to channel B. The result was an anomaly of the type shown in the right-hand side of figure 2, implying that the gap correction was too large.

The same input signals were reprocessed using a slightly smaller gap correction for channel A. The result is shown in figure 3. The feature between the third and fourth tick marks is due to the channel A midscale problem, and the feature between the fourth and sixth tick marks is due to the channel B midscale problem. Examining the channel A feature more carefully, it can be seen that there is gap-induced anomaly (as shown in the left side of figure 2) which arises because the gap correction is now too small, superimposed on a broader anomaly, caused by a flat spot in the return (as shown in the right side of figure 2). Since the crossover adjustment has been set to produce a gap in the return, it cannot also produce a flat spot in the return. Therefore, the flat spot is caused by something else. The most likely source is a small nonlinearity in the folding amplifier when the input signal is near zero.

The tests just described have demonstrated problems which are associated with the point where the input signal crosses zero. The first is

the sensitivity of the crossover adjustment. The second is a slight nonlinearity, probably in the folding amplifier. The crossover adjustment problem, while annoying, is not insurmountable, since it can be corrected analytically.

The second problem, however, is more serious and would be quite difficult to correct. It should be pointed out that the nonlinearity at the zero crossing point is a very small effect and in most applications is not detectable. However, the differential absorption calculation is very sensitive to nonlinearities. Therefore, for differential absorption applications, the input signals should be restricted so that they are always positive or always negative, thus avoiding the problems at the zero crossing point. This reduces the dynamic range from eight to seven bits so it may be necessary to average more returns to get acceptable accuracy.

The tests described above were repeated with the input signals strictly greater than zero. The calculated concentration showed no systematic anomalies.

The second transient digitizer studied was the Biomation model 1010. This digitizer can sample an analog input wave form at intervals as short as 100 ns, convert the analog samples to digital form, and store the samples in a 2050-word memory. The digital resolution of this unit is 10 bits or 1 part in 1024. The input signal passes through the input amplifier which consists of two identical stages, each preceded by an attenuator section to provide the various input ranges, and then to the analog to digital converter. The analog to digital converter is a dual-rank type, or two parallel comparator converters in series. The first parallel comparator converter determines the five most significant bits of the digital result, and the second parallel comparator converter provides the five least significant bits.

The performance of the Biomation 1010 digitizer was investigated using a decaying exponential signal to simulate a lidar return. The model 1010 is a single channel device, so two-channel operation was simulated by treating the even-numbered words of the digitized signal as the on-line return and the odd-numbered words as the off-line return. As before, 100 wave forms were averaged and the concentration calculated with the on-line data shifted

with respect to the off-line data so that any systematic errors would show up. The result showed no systematic error which could be attributed to the transient digitizer.

There are two primary conclusions to be drawn from this study. The first is that for sampling intervals of 100 ns or greater the Biomation model 1010 or a similar unit should be used for differential absorption measuremonts. Second, if sampling intervals shorter than 100 ns are required, the Biomation model 8100 can be used, but input signals must be either strictly positive or strictly negative in order to avoid the error at the zero crossing point.

3. UV DIAL SYSTEM

The UV DIAL system is being developed for the remote investigations of SO_2, O_3, and aerosols present in power plant and urban plumes. The data obtained will be used together with that from other sensors in dispersion, transformation, and deposition studies. It is important to know what happens to the SO_2 because of the potential health and environmental effects of sulfur compounds. In addition, these studies will allow the reassessment of the accuracy of current plume models in predicting the temporal and spatial changes in pollutant concentrations and compositions. It is important to study O_3 because of its role in photochemistry and its potential adverse effects on health and vegetation in large concentrations (greater than 50-100 ppb).

Development efforts during the past year have been primarily with the laboratory SO_2 lidar system operating near 300 nm. Future plans are to "harden" the system for use in the field and aboard an aircraft, and to develop the system capabilities for O_3 investigations around 283 nm.

The system uses a double-pulse frequency-doubled Neodymium-doped yttrium-aluminum garnet (Nd:YAG) laser as a pump for two independent dye lasers. This concept, developed by Dr. Browell at NASA/LaRC (ref. 7), allows the transmission of two closely spaced sequential laser pulses at two different wavelengths (300.2 nm and 299.5 nm) for SO_2 differential absorption observations. In addition, the system produces an output at 600.4 nm for aerosol backscattering observations. The DIAL concept

will now be described qualitatively. This section will be completed with a description of the UV DIAL system

3.1. UV DIAL Concept

(See reference 1.) The Differential Absorption Lidar (DIAL) has become a primary method for remote measurement of gases in the troposphere. To accomplish this, pulsed laser radiation at two wavelengths is transmitted into the atmosphere. The two wavelengths are selected so that one, called the on wavelength, is absorbed by the gas of interest, while the other, called the off wavelength, is not. The backscatter return signal as a function of range at each wavelength is collected by an optical receiver. Now define a range cell as the distance from R_1 to R_2. The average concentration of the absorbing gas in the range cell may be determined from the on and off wavelength returns at R_1 and R_2. The situation is analagous to a dual-beam spectroscopy experiment where the off wavelength return corresponds to the reference beam, the on wavelength corresponds to the sample beam, and the range cell corresponds to the sample cell. The transmittance of the absorbing gas in the range cell is then just the ratio of the on wavelength returns at R_2 and R_1 divided by the ratio of the off wavelength returns at R_2 and R_1.

The quantitative expression for absorber concentration can be found using the lidar equation:

$$P_r(R,\lambda,t) = K \frac{L}{2} \frac{A}{R^2} P_o(\lambda)\, \beta(R,\lambda,t) \cdot \exp\left\{-2\int_o^R \left[\alpha_{sc}(r,\lambda,t) + N_A(r,t)\sigma_A(\lambda,P,T) + N_{int}(r,t)\sigma_{int}(\lambda,P,T)\right] dr\right\} \quad (2)$$

Here P_r is the received power as a function of range R, wavelength λ, and time t; K is a constant; L is the laser pulse length; A is the receiver area; $P_o(\lambda)$, the transmitted power, is a function of wavelength; β is the backscatter cross section as a function of range, wavelength, and time; α_{sc} is the extinction coefficient for scattering as a function of range, wavelength and time; N_A is the concentration of the absorbing gas of interest as a function of range and time; σ_A is the absorption cross section of the gas of

interest as a function of wavelength, pressure, P, and temperature, T; N_{int} is concentration of any interfering absorbing gas; and σ_{int} is the absorption cross section of the interfering gas.

A number of assumptions are made to simplify the analysis. The scattering terms are assumed equal for the on wavelength and the off wavelength returns, that is $\beta(R,\lambda off,t\ off) = \beta(R,\lambda on,t\ on)$ and $\alpha_{sc}(R,\lambda off,t\ off) = \alpha_{sc}(R,\lambda on,t\ on)$. Also, the concentrations of the absorbing and interfering gases are assumed to remain constant between the off wavelength and on wavelength returns, that is, $N_A(R,t\ off) = N_A(R,t\ on)$ and $N_{int}(R,t\ off) = N_{int}(R,t\ on)$. The on and off wavelength absorption cross section for the gas of interest $\sigma_A(\lambda off,P,T)$ and $\sigma_A(\lambda on,P,T)$, are assumed to be known and constant between R_1 and R_2. If $\sigma_{int}(\lambda off,P,T)$ is not equal to $\sigma_{int}(\lambda on,P,T)$, then both the concentration and absorption cross section of the interfering gas must be known or must be determined by a separate experiment.

With the above assumptions the average concentration of N_A of the gas of interest in the range cell between R_1 and R_2 is

$$NA = \frac{1}{2(R_2 - R_1)\left[\sigma_A(\lambda on) - \sigma_A(\lambda off)\right]} \ln\left[\frac{Pr_{on}(R_1) \times Pr_{off}(R_2)}{Pr_{off}(R_1) \times Pr_{on}(R_2)}\right] \qquad (3)$$

The small separation in time (less than 100 μs) of the on and off wavelength pulses in the UV DIAL transmitter minimizes errors in the measured concentration which might arise from time variations of β and α_{sc}. The time separation also allows the receiver electronics to be time multiplexed, with the same photomultiplier and transient digitizer being used for both the on and off wavelength returns, thus eliminating another potential source for systematic error.

The DIAL technique was first used by Schotland (ref. 8) to measure water vapor. Subsequent remote measurements of NO_2 (ref. 9), SO_2 and O_3 (ref. 10) have been made by other investigators using this method.

3.2. Description of the UV DIAL System

The UV DIAL System consists of a trilaser transmitting system, a dual-photomultiplier multiplexed receiver, data processing subsystem, and

associated timing/control logic. The transmitter uses an International Laser System (ILS) double-pulsed frequency-doubled Nd:YAG laser as a pump for two dye lasers, each tuned to a slightly different wavelength. The ILS laser, designed to NASA specifications, produces a pulse-pair (pulse A and pulse B) transmitted at a wavelength of 532 nm sequentially at time t_o and $(t_o + \Delta t)$ where $90 \leq \Delta t \leq 99$ μs. The energy contained in each pulse is about 150 mJ with a maximum prf of 5 Hz.

Pulses A and B are directed either to an off-line or an on-line dye laser by an optical switch consisting of a Pockels cell, dielectric polarizer and half-wave plate (see figure 4). If the applied voltage to the Pockels cell crystal is zero, the horizontally polarized pulse from the ILS laser will pass through the cell unaffected and be directed to the off-line dye laser by the dielectric polarizer. When a high-voltage pulse is applied to the Pockels cell, the transmitted polarized light is rotated 90°, thereby being directed by the dielectric polarizer to the on-line cavity. A half-wave plate is inserted to rerotate the light back to its original horizontal polarization. A switch S-1 has been added to the Pockels cell control electronics that will allow the option to open the Pockels cell at time t_o or at time $(t_o + \Delta t)$, thereby routing pulse A either to the on-line or the off-line dye laser respectively. This is summarized in table 1.

Table 1. Optical switch pulse routing, off- or on-line dye laser.

Switch S-1 Position	Pockels Cell Open at Time:	Pulse Directed to	
		On-line Laser	Off-line Laser
A on-line	t_o	A	B
B on-line	$t_o + \Delta t$	B	A

The components in both dye lasers are identical. These consist of a beamsplitter, oscillator and amplifier dye cells, an oscillator cavity output mirror, and a 79-grove/mm echelle grating. The beamsplitter divides the green wavelength energy transmitting about 45 mJ to pump the oscillator cell and reflecting 105 mJ to pump the amplifier cell. The dye is

circulated through all four cells in series* and consists of a 1.5×10^{-4} molar concentration of Kiton Red S dye dissolved in water with 3 percent Ammonyx LO, which makes the solution slightly basic. The dye cavities are presently tunable over a range from about 585 nm to 615 nm by the echelle gratings. The on-line cavity is nominally tuned to 600.4 nm and the off-line to 599 nm for SO_2 observations. The dye will be changed and probably circulated through only two cells in the on-line laser for optimum operation at 566 nm for the future O_3 observations. By using the dye amplifiers, the oscillator output energy is increased to 25 mJ with a line width of 0.04 nm.

The horizontally polarized output from each of the two dye lasers is individually directed through two temperature-tuned ADA frequency doubling systems. The ADA crystals double the dye laser wavelength into the UV with about 10 percent conversion efficiency producing about 2.5 mJ of UV and about 22.5 mJ of the fundamental. A dichroic beamsplitter following the doubler passes the fundamental for propagation into the atmosphere and reflects the second harmonic through the beamsplitter/mirror arrangement shown in figure 4.

The beamsplitters in the UV primary paths direct a small portion of the UV energy to a SO_2 absorption cell assembly. Two adjustable irises are mounted on the two input apertures (for pulses A and B) located on the side and end of a black cover box. A beamsplitter, absorption cell, diffusers, UV neutral density filter, and two photodiodes are mounted inside the area covered by the box. The arrangement of these components is shown in figures 5 and 6 The UV energy from each pulse is directed by the beamsplitter so that approximately one-half the energy is directed through the absorption cell to the photodiode labeled g_{DT}, while the remaining energy bypasses the cell and is directed to the photodiode labeled g_{DB}. This arrangement together with the calibration and normali-

---

* Studies were conducted to determine the optimum dye concentration as a function of power out of the dye oscillator cavity and amplifier. It was found that there was only a slight decrease (6%) in output power by using the same dye concentration and circulating the dye in series within all four dye cells. It was felt that the simplified dye-circulating system warranted the sacrifice in power at this time.

zation process discussed below provides a means for measuring the absorption coefficient, $\sigma(\lambda)$, with each lidar shot and accounting for uncertainities in wavelength, λ.

3.3. Absorption Cell Theory

Figure 5 shows the optical path when the UV off-line pulse enters the side of the absorption cell assembly; Figure 6 shows the on-line pulse entering the end of the absorption cell assembly. These two could be interchanged by the t_o - (t_o + t) switch on the Pockels cell control unit as discussed earlier in this report.

From Figure 5 we can write,

$$V_3(t) = I_{off}(t)\, R_{off}\, T_c\, T_g(\lambda)\, T_{FT} g_{DT} G_{AT} + dc_{offset} \tag{4}$$

and

$$V_4(t) = I_{off}(t)\, T_{off}\, T_{FB}\, g_{DB} g_{AB} + dc_{offset} \tag{5}$$

Likewise Figure 6 produces

$$V_1(t') = I_{on}(t')\, T_{on}\, T_c\, T_g(\lambda)\, T_{FT} g_{DT} g_{AT} + dc_{offset} \tag{6}$$

$$V_2(t') = I_{on}(t')\, R_{on}\, T_{FB} g_{DB} g_{AB} + dc_{offset} \tag{7}$$

and

$$t' = t_o + \Delta t \tag{8}$$

where I(t) and I(t') are the intensities of the UV laser beams, after passing the iris, R represents the reflectance and T the transmittance of the beamsplitter, and $T_c(\lambda)$, $T_g(\lambda)$, and $T_{FT}(\lambda)$ represent the transmittance of the empty cell, absorbing gas, and filters, respectively. The terms g_D and g_A are the transfer characteristics KG(jw) of the detectors and amplifiers (quad-integrator) respectively. The dc_{offset} term is the combined dc offset from the battery and drift within the amplifier, which

is minimized by capacitance coupling and calibration of the quad-integrator. The second subscripts T and B represent the path through and the path by-passing the cell respectively. The transmittance of the gas within the cell can be further defined by

$$T_g(\lambda) = e^{-\sigma LP} \tag{9}$$

where L is the path length of the absorbing gas in cm, P is the gas pressure in atmospheres, and σ is the absorption coefficient in $(atm\text{-}cm)^{-1}$.

In order to obtain an expression for $\sigma(\lambda)$ which is independent of the system's parameters, calibration constants, $C(\lambda)$, are obtained with no gas in absorption cell by taking the ratio of the "through cell" signal to the "bypass cell" signal. When $T_g(t) = 1 = T_g(t')$ and the $dc_{offset} = 0$,

$$C_{off}(t,\lambda) = \frac{V_3(t)}{V_4(t)} = \frac{R_{off}\, T_c\, T_{FT}\, g_{DT} g_{AT}}{T_{off}\, T_{FB}\, g_{DB} g_{AB}} \qquad \text{cell empty} \tag{10}$$

$$C_{on}(t',\lambda) = \frac{V_1(t')}{V_2(t')} = \frac{T_{on}\, T_c\, T_{FT}\, g_{DT} g_{AT}}{R_{on}\, T_{FB}\, g_{DB} g_{AB}} \qquad \text{cell empty} \tag{11}$$

The absorption cell is constructed with a cold finger as shown in figure 7. During the calibration run to determine $C(\lambda)$, the cold finger is immersed in liquid nitrogen which condenses all the SO_2 in the cell. Following the calibration run, the liquid nitrogen is removed and the cold finger is allowed to return to room temperature. This allows the SO_2 to return to the path of the UV laser beam which will make $T_g < 1$.

To determine the transmittance of the gas within the cell, the constants determined by equations (10) and (11) are multiplied by the ratio of the bypass cell signal to the through cell signal. Expressed mathematically,

$$T_g(t,\lambda) = C_{off}(t,\lambda)\, \frac{V_4(t)}{V_3(t)} \qquad \text{cell thawed} \tag{12}$$

and

$$T_g(t',\lambda) = C_{on}(t',\lambda)\,\frac{V_2(t')}{V_1(t')} \qquad \text{cell thawed} \qquad (13)$$

The absorption coefficients for the off-line and on-line are then determined using equation (9), and the wavelength is determined from a plot or table of absorption coefficients versus wavelength. The above analysis is based upon the assumptions that (1) the $dc_{offset} = 0$ and remains 0 during the experiment, and (2) the wavelength at the time of determining $C(\lambda)$ is the same as when measuring $T_g(\lambda)$.

3.4. Timing and Control

The timing and control are illustrated in figure 8 along with the outputs from the photodiodes installed within the Nd-Yag laser and SO_2 absorption cell assembly. The firing rate is controlled by a Berkeley Nucleonics Corp (BNC) model 8010 pulse generator #1. The complement positive output pulse is supplied to the EXTERNAL input jack of the ILS HL-101 laser and commands the laser to fire on its negative transition (t_1). Logic and delays within the ILS laser result in the following sequence of signals with Δt set to 90 μs and the DIP switches, or the flashlamp to Pockels cell command delay set to binary 61, which is 97 μs:

t_1 + 2 μs - command to fire all three flashlamps

t_1 + 92 μs - command to fire all three flashlamps a second time

t_1 + 100 μs - leading edge (positive transition) of 30 μs pulse produced on BNC output jack labeled MONITOR PULSE 1 = t_o - 2 μs

t_1 + 100 μs - command to open Pockels cell and laser

t_1 + 102 μs - laser pulse A transmitted = t_o

t_1 + 190 μs - leading edge (positive transition) of 30 μs pulse produced on BNC output jack labeled MONITOR PULSE 2 = t_o + 88 μs

t_1 + 192 μs - laser pulse B transmitted = $t_o + \Delta t = t_o$ + 90 μs

The monitor pulse #1 is used to trigger pulse generator #3 which outputs a 100-ns wide gate pulse with a transition from -0.5 V to -1.5 V required to be compatible with the ECL (Emitter Coupled Logic) used within the LeCroy

Research Systems (LRS) model 227 quad integrator unit. This negative pulse is used to "gate on" channels 1 and 2 of the quad integrator starting at (t_o - 40 ns) and ending at (t_o + 60 ns). This will allow for a maximum of ±40-ns jitter* of the 20-ns wide t_o pulse within the 100-ns gate. One hundred ns is the maximum gate duration recommended by the quad integrator manufacturer in order to obtain the specified linearity (±0.4% of reading, ±0.2% of full scale) of integration. In addition, a narrow gate minimizes errors in the output due to the integration of noise on the signal line before and after the t_o pulse.

The monitor pulse #2 triggers pulse generator #4, which produces a 100-ns wide gate pulse used to gate on channels 3 and 4 of the quad integrator. The delay time of this gate is set by front panel controls on pulse generator #4 starting at (t_o + Δt - 40 ns) and ending at (t_o + Δt + 60 ns).

The quad integrator outputs four voltages to the computer: V_1 and V_2 are the integrated t_o outputs from the through and pass absorption cell photodiodes respectively, and V_3 and V_4 are the (t_o + Δt) outputs from the through and pass absorption cell photodiodes respectively. These signals are processed by the computer as discussed in "Absorption Cell Theory."

Pulse generator #2 is provided to furnish a Reset signal to the quad integrator and provide an advance pulse to the computer through a line driver. Both of these early pulses are provided at time t_1. In addition, the computer is provided t_o and (t_o + Δt) through a signal conditioning and line driver module. These pulses are generated by a photodiode sensing the 532-nm laser power envelope installed within the ILS laser pump.

A voltage converter is coupled to pulse generator #1 to provide an 18-V pulse to trigger a Holobeam model H-11 Pockels Cell Q-switch control unit. This unit produces a -13 KV pulse starting at time t_2, which is adjusted (by a potentiometer on the control unit) so that the Pockels cell (part of the optical switch) is fully open at time (t_o + Δt) when switch S-1 is in the B on-line position. When switch S-1, located on the Pockels cell control unit, is placed in the A on-line position, the -13 KV pulse

---

* The jitter was measured to be less than ±30 ns.

is repositioned ahead of t_o so that the Pockels cell is fully open at time t_o. Switch S-1 then directs pulse A to either the off-line or the on-line dye laser.

A block diagram of the receiver system is shown in figure 9. The receiver consists of a 30-cm Cassegrain telescope with UV-enhanced coatings on the primary and secondary mirrors, and a detector package. In the detector package a dichroic beamsplitter is used to separate the backscattered UV radiation near 300 nm from the backscattered visible radiation at 532 nm or 600 nm. The UV radiation is detected using an RCA C7268 photomultiplier tube which has the same dynode structure as an RCA 7265 photomultiplier but with a bialkili photocathode for enhanced UV quantum efficiency. The visible radiation is detected using a standard RCA 7265 photomultiplier tube. The gain of the photomultiplier tubes can be modulated so that it is proportional to t^2, where t is time (ref. 11). This compensates for the $\left(\frac{1}{R}\right)^2$ dependence of the return signal and reduces the dynamic range of the signal.

The signals from the photomultiplier tubes are fed to Biomation wave form recorders where they are converted to digital form. The digitized return signals are then read by the PDP 11/10 minicomputer and recorded on magnetic tape for later processing. The PDP 11/10 is programmed so that data analysis can proceed simultaneously with data recording. This permits preliminary analysis and display of the data in nearly real time so that operation of the system can be monitored and changed if necessary. The data acquisition system is the same as that used for the plume dispersion study and is described in more detail in Section 5.

4. IR DIAL SYSTEM

The infrared region of the spectrum from 1.5 to 4.5 μm contains fundamental, combination, and overtone bands of a number of tropospheric pollutant and trace gases. The objective of this program is to develop a mobile DIAL system which would have the capability of making remote measurements of many of these gases with particular emphasis on effluents in power plant plumes.

Development of the system has been delayed by difficulties encountered by the laser supplier. However, progress has been made in assembling and testing other components of the system and in analytical studies to determine operating wavelengths and expected sensitivities for some of the gases of interest.

The most critical component of the system is the laser transmitter because it must have high power, tunability, and narrow line width. The laser is being developed by Westinghouse Research Laboratories under contract to NASA Langley Research Center, and is based on technology demonstrated at Stanford University (ref. 12). A schematic of the laser transmitter is shown in figure 10. A Nd:YAG oscillator and amplifier is used to pump an Optical Parametric Oscillator (OPO) and Optical Parametric Amplifier (OPA). The oscillator produces 150 mJ/pulse at 10 Hz with 0.1-cm^{-1} line width from an unstable resonator cavity. The amplifier then increases the oscillator energy to 350 mJ/pulse. Approximately 60 mJ of the 1.06 μm energy are used to pump the OPO, and the remaining energy is used to pump the OPA. Angle tuned $LiNbO_3$ crystals are used in the OPO and OPA for the nonlinear conversion of 1.06-μm energy to tunable IR energy. One of the requirements for wavelength conversion is $\omega_p = \omega_s + \omega_i$, where ω_p is the pump frequency, and ω_s and ω_i are the signal and idler frequencies, respectively. The signal wavelength is oscillated in the OPO cavity, and line narrowing is accomplished by a grating and etalon to achieve a line width in both signal and idler wavelengths of 0.1 cm^{-1}. The OPA increases the output of the OPA at 2.2 μm to a total of 50 mJ/pulse in the signal and idler wavelengths. For DIAL measurements the OPO grating is rocked between modes of the etalon to produce alternating on/off signal and idler wavelengths. Discrimination between the signal and idler wavelengths is accomplished by filters in the receiver.

The receiver system consists of a 46-cm diameter, gold-coated Newtonian telescope and liquid-nitrogen cooled, 1-mm diameter InSb detector. The laser beam must be transmitted coaxially with the telescope since the laser divergence is less than 0.4 mrad and the telescope field of view as determined by the detector size is 0.8 mrad. This is accomplished using a Coudé mount for the telescope so that the laser remains stationary and the laser beam is directed along the axes of rotation of the mount and then

coaxial with the telescope. An absorption cell with path length adjustable up to 200 m will be used to measure the absorption coefficient of the gas being measured for each laser pulse. Detectors for use with the absorption cell have been tested to determine their linear region of operation, and a gas-handling system for the absorption cell has been designed and built. The data acquisition system is similar to that used for the UV DIAL system.

Available spectroscopic data have been used to make preliminary estimates of the measurement capability of the system for various gases. These estimates are shown in table 2 assuming a five percent uncertainty in measuring the transmittance. Improved sensitivity could be obtained by averaging laser shots. The system should have fairly high sensitivity for measuring HCl, CH_4 and H_2O. The relative insensitivity of the system for measuring SO_2 limits its application to near stack exit conditions. The UV DIAL system is restricted to measuring concentrations of SO_2 which are less than 300 ppm over a 10-m distance because of residual absorption by SO_2 at the off-wavelength, and therefore will be applied to measurements of SO_2 at large distances from stacks and in regional investigations. The lower sensitivity of the IR DIAL system thus complements the UV DIAL system in the measurement of SO_2.

Table 2. Estimated IR DIAL Sensitivities.

Species	Wavelength μm	Optical Depth Sensitivity ppm - meter
SO_2	4.0	540
CO	2.33	660
HCl	3.54	25
CH_4	3.27	5.3
CO_2	2.06	7400
H_2O	Selectable	Selectable
N_2O	3.88	280

5. POWER PLANT PLUME DISPERSION STUDY

In early 1976 an agreement was made by NASA/LaRC and the Power Plant Siting Program of the State of Maryland Department of Natural Resources (PPSP) to perform a joint experiment to determine the utility of the lidar as a method for characterizing plume rise and plume dispersion from large fossil fuel burning power plants. The experiment was conducted during four one-week periods during September and October 1976. In this section the design and results of that experiment will be described. Some of the material in this section has been presented before (refs. 1, 4); however, it will be repeated here for completeness.

The Power Plant Siting Program is responsible for determining the environmental impact of proposed power plants and for maintaining an inventory of environmentally suitable sites which can be acquired by a utility or exchanged for a site a utility owns which has been determined to be environmentally unacceptable. As an aid to improving the validity of environmental impact statements, PPSP has contracted with Martin Marietta Research Laboratories (MML) and Environmental Measurements Inc. (EMI) to perform a fairly extensive theoretical and experimental study of plume dispersion from tall stacks with the objective of improving existing plume rise and plume dispersion models, or developing new models if existing models prove to be inadequate.

There were a number of organizations in addition to NASA/LaRC and PPSP who made contributions to the joint experiment. The experiment was conducted at the Morgantown Generating Plant of the Potomac Electric Power Company. Personnel at the plant were very cooperative in terms of providing information on operating conditions of the plant and providing space and facilities for making some of the measurements. MML served as a contact with the power company and PPSP and coordinated the activities of the various groups in the field. EMI performed a major role in the experiment, making meteorological measurements and conventional plume measurements. Radiosondes were launched three times a day to measure the temperature profile. In addition, pilot balloons were released every hour to measure wind speed and direction as a function of altitude. EMI plume measurements were made using two instrumented vans: one, the Air Quality Moving Laboratory (AQML),

measured total integrated SO_2 overhead using a Barringer correlation spectrometer and in situ SO_2 concentration as it traversed beneath the plume on available roads. The second van, the Transportable Laboratory (TPTL) was positioned near the plume centerline in an area where the plume was touching down and measured in situ SO_2 concentration on a time-averaged basis. Engineering-Test Services (ETS) made in-stack measurements of the mass emission rate, SO_2, total particulates, and particle size distribution. Lidar measurements of plume rise, plume dispersion, and mixing layer height were made by Old Dominion University and Wyle Laboratories. Lidar data reduction and analysis were performed by ODU using the NASA/LaRC computer facilities.

The joint experiment was designed by a group which included the investigators making the measurements and modelers and data analysts from NASA/LaRC, MML, Goddard Institute for Space Studies, and ODU. The results of a simulation of the lidar experiment performed by Kibler (ref. 13) were used as a guide for selecting suitable sites for lidar operation and for developing the optimum lidar data taking strategy.

5.1. Mobile Lidar System

The mobile lidar system was built by personnel from ODU, NASA, and Wyle Laboratories using NASA equipment. A block diagram of the system is shown in figure 11. The lidar system consists of a ruby laser, a telescope receiver, a detector package, and associated instrumentation. The laser, telescope, and detector package are mounted on a searchlight mount with tracking capability. The entire system, including instrumentation and the searchlight mount, is contained on a flatbed trailer.

The laser used in the system is a Holobeam 600 Q-switched ruby laser with a beam divergence of 3½ mrad. The beam divergence was reduced to approximately 1 mrad by using an up-collimating telescope at the output of the laser. The output energy of the laser can vary from 0.75 to 2.0 J per pulse with a pulse length of 30 ns and a pulse repetition frequency up to 1 pulse per second. The ultimate range resolution attainable is 4.5 m.

The receiver is a 30-cm cassegrain type telescope with a field of view of approximately 4 mrad. The detector package has a provision for mounting two photomultiplier tubes for extended dynamic range. For the plume dispersion experiment, only one tube was used. An RCA 7265 photo-

multiplier tube was selected for use in the system since it is sensitive to the 694-nm laser radiation, and it could be easily gated to prevent overload from the close-in return.

The instrumentation used consists of a high voltage power supply and gating circuit for the photomultiplier tube, pulse generators used for timing, and the data acquisition system.

The data acquisition system is based on a Digital Equipment Corporation model PDP 11/10 minicomputer. The lidar return signal from the photomultiplier passes through a log amplifier and is recorded by a Biomation model 8100 transient digitizer which can record 2048 8-bit words of data at sample rates up to 100 MHz. The log amplifier reduces the dynamic range of the signal to the transient digitizer. The transient digitizer has an analog output so that the data can be displayed continuously on an oscilloscope and a digital output from which the computer accepts the recorded data. Other data accepted by the computer include laser energy, laser shot counter reading, and elevation and azimuth angle from the searchlight mount. The data from each laser firing is immediately recorded on magnetic tape for later processing using either the PDP 11/10 or the main Langley Research Center computer facility. Also attached to the minicomputer is a Ramtek graphics display generator which can display information in 16 shades of gray on a standard black and white television monitor.

The computer has been programmed to allow data processing to proceed simultaneously with data recording. This permits preliminary data analysis (such as range correction) and display on a nearly real-time basis. Three different types of data display are available: one is called an A-scope display and is simply an X-Y [illegible]ith no intensity modulation of the display. Another type of display, called a Z-scope display, is useful for applications where the lidar is pointed vertically, such as in mixing layer height measurements. This display plots intensity versus height on a vertical line using the 16-shade gray scale modulation. The third type of display is the RHI or range, height, intensity display which is used for displaying plume dispersion lidar returns. For this display, the horizontal axis corresponds to the horizontal distance from the lidar and the vertical axis corresponds to height above the lidar. Intensity is then plotted along a line which corresponds to the lidar elevation.

The maximum range of the lidar is not known. However, in this experiment measurements of plumes were made up to nine km from the power plant and up to nine km from the lidar.

The Morgantown power plant is located on the Potomac River in Charles County, Maryland about 56 km (35 mi) south of Washington, D.C. where U. S. Route 301 crosses the Potomac River. The plant has two 575-MW generating units operating on coal or oil or a mixture of both. During the time when this experiment was conducted, the fuel mix was approximately half coal and half oil. Flue gases are exhausted through two 213-m stacks located 76 m apart. The stack exit velocity is 30-m/s and the stack exit temperature is 135°C. For the two one-week measurement periods in September, both generating units were operating. However, for the two one-week periods in October, one unit was shut down for maintenance, so only one unit was operating.

Figure 12 shows a map of the area around the power plant with the lidar sites used indicated by stars. Circles centered at the power plant with one-km increments of radius are drawn on the map for reference.

The basic measurement strategy was to locate the lidar two to four km from the plant at a site selected so that the plume could be viewed from the side. Cross sections of the plume were obtained by scanning the lidar vertically through the plume at selected downwind distances from the stack. The measurement sequence was repeated several times over a one-hour period in order to obtain time-averaged measurements. Where possible, one of the downwind distances was selected to coincide with simultaneous measurements made by EMI using the AQML. Lidar measurements of mixing layer height were made before and after each series of plume measurements.

Because of the time required to relocate the lidar (approximately six hours) and the potential electronic malfunctions which could be caused by moving, a lidar site was chosen for several days of operation even though it might not be ideal for every day. The site chosen was based on the weather forecast from the National Weather Service. As it turned out, one site was used for each one-week measurement period. For the period from September 7-10, 1976, the lidar was located at site number 1 indicated in figure 12 at a distance of 1.91 km and bearing 74° from the north stack of the power plant. From September 20-24 the lidar was located at site

number 2, 3.12 km from the north stack at a bearing of 145°. From October 11-15 the lidar was located at site number 3, 3.84 km from the north stack at a bearing of 5.8°. From October 25-29 the lidar was located at site number 4, 3.54 km from the north stack at a bearing of 261°.

Data reduction and analysis were performed using the LaRC computer facility.

5.2. Data Reduction Techniques of Lidar Plume Measurements

The returns are initially corrected for a system offset and log amplification. The offset is required due to inherent limitations of the log amplifier. Actual amplification differs from the true log function, so calibration techniques were used to determine a log transfer function. These corrections to the lidar signal are combined in the following equation:

$$V'(R) = 5.8063 + 0.0337\ V(R) - 0.00004\ V^2(R) \qquad (14)$$

A background return is obtained by gating on the photomultiplier tube without firing the laser. This signal represents ambient light entering the tube as well as electronic noise. Since the background return is fed through the log amplifier it must also be corrected by equation (14).

Once the plume and background returns are corrected, the background is subtracted and the result is range corrected by R^2 where range (in km) is determined as follows:

$$R_i = 0.15\ (\tau + 1/f) \qquad i = 1,2024$$

τ = initial delay (μsec)

f = sampling frequency (MHz) (15)

The range resolution for a sampling frequency of 50 MHz is then 3 m. Altitude (Z) and horizontal distance from the lidar (Y) are calculated using the elevation angle (θ):

$$Z = \sin(\theta) + Zsl \tag{16}$$

$$Y = \cos(\theta) \tag{17}$$

Zsl = altitude above sea level of lidar.

After correcting the raw data for log amplification, background and range, the resulting profiles represent relative measurements of the attenuated aerosol and molecular atmosphere along the lidar line of sight. To eliminate the attenuation effects, a profile of the molecular atmosphere is usually employed to normalize the lidar returns. Since a molecular profile was not available, a portion of the lidar return, prior to the plume and extrapolated on out, was chosen to represent the ambient atmosphere. Due to spurious tails introduced by misalignment of the lidar system, a quadratic fit is used. The limits of the curve fitting are specified and are constant for any set of scans at one particular azimuth angle. The lidar profiles are then divided by the fitted curve to yield ratios of plume to nonplume data. The curve-fitting limits are chosen (by trial and error) to produce ratios close to unity for nonplume portions of the profile. In some cases, the curve had to be fitted to sections of the profile both before and after the plume to obtain these results. Truncation is necessary in some cases at one or both ends of the profiles. To obtain relative magnitudes of only the plume, one is subtracted from all ratios, and any results less than zero are set equal to zero.

Grid limits are chosen so as to center the plume in both the Y and Z planes. Profiles are placed in the grid, and where several data points fall within the same grid box an average value is computed. Interpolation is performed on any empty grid box adjacent to a nonempty grid box using the four adjacent boxes. A negative sign is attached to interpolated points to differentiate them from actual values. The value of -999.0 is placed in all remaining empty boxes to indicate lack of data rather than lack of plume.

The total burden of a scan is calculated by summing all actual and interpolated points in the grid. If the lidar measure of the plume is denoted by S then the total burden (S_t) is:

$$S_t = \sum_Y \sum_Z S \tag{18}$$

The centroids ($\bar{Y}$ and $\bar{Z}$) and their deviations (σ_Y and σ_Z) are defined by

$$\bar{Y} = \left(\sum_Y \sum_Z S\,Y\right)/S_t \tag{19}$$

$$\bar{Z} = \left(\sum_Y \sum_Z S\,Z\right)/S_t \tag{20}$$

$$\sigma_Y = \left(\sum_Y \sum_Z (SY^2)/S_t - \bar{Y}^2\right)^{1/2} \tag{21}$$

$$\sigma_Z = \left(\sum_Y \sum_Z (S\,Z^2)/S_t - \bar{Z}^2\right)^{1/2} \tag{22}$$

The rotation correction (a) previously mentioned and the centroid distance downwind ($\bar{X}$) are determined as follows:

$$\bar{X} = \left(L^2 + \bar{Y}^2 - L\,\bar{Y}\,\cos(\phi)\right)^{-1} \tag{23}$$

$$a = \cos\left\{\pi/2 - \cos^{-1}\left[\left(\bar{X}^2 + \bar{Y}^2 - L^2\right)/(2\,\bar{X}\,\bar{Y})\right]\right\} \tag{24}$$

where L is the distance of lidar from the smokestack and ϕ is the azimuth angle of scan.

Two types of averages were calculated for a set of scans at a given azimuth angle: an Eulerian average and a Lagrangian average. For the Eulerian plume average, grid points, including interpolated values, are averaged over a set of scans at the same azimuth angle. No further interpolation is performed. The values of S_t, $\bar{Y}$, $\bar{Z}$, σ_Y, σ_Z, $\bar{X}$ and a are then recalculated for the averaged scan exactly as before.

For the Lagrangian plume average the individual grids are averaged together by superimposing the centroids. The new grid is related to the original grids by the following:

$$Y' = (Y - \bar{Y})\,a \tag{25}$$

$$Z' = (Z - \bar{Z}) \tag{26}$$

The values of interest are again recalculated in a similar manner as before with the following exceptions:

(1) The rotation correction is eliminated from equation (19) since it has already been accounted for in equation (25).

(2) The value of $\overline{Y}$ in equation (23) is an average of the Y centroids on the individual scans. The Y centroid on the Lagrangian average should be zero, but due to the shifting of the new grid this is not usually the case.

(3) The rotation correction is not calculated in equation (24) since individual grids are rotated prior to placement in this averaged grid [eq. (25)].

Once the grids representing individual scans and averages of scans are created, a number of other calculations can be made and the results plotted or presented in tabular form.

The grid is divided into 10 equally spaced vertical and horizontal slices. The following computations are then made:

(1) Maximum S within the slice (plots 1 and 6) and its corresponding Y value (plot 2) or corresponding Z value (plot 7).

(2) Line integrals determined by summing all values of S within a horizontal slice (plot 3) or within a vertical slice (plot 8).

(3) The variation of the centroid and its deviation versus altitude (plot 4) and versus distance from the lidar (plot 9).

Plots 5 and 10 represent slices up the centroids of the plume and the normal curve computed from the mean and standard deviation. The slices on these two plots are of the same resolution as the grid, which at present is 20 m.

In addition, a contour plot is available for each individual and each averaged grid.

A magnetic tape has been generated which contains all the lidar plume data obtained in the experiment. The data is recorded in the form of the grids described previously.

Each grid is contained in a separate file which consists of a header record, the grid, and end of file mark. The information in the header record is tabulated in table 3. The number of points in the grid are stored in words 22 and 25. The grid was placed on tape with the following implied do-loop:

```
JTOT = HDR(22)                          (Z - plane)
ITOT = HDR(25)                          (Y - plane)
((S(I,J), I = 1, ITOT), J = 1, JTOT)
```

The entire tape is written with a 10E10.3 format. There are a total of 423 grids (either individual or averaged) on the tape from the Morgantown study.

A copy of the data tape and the plots and tables described, as well as the meteorological data and conventional plume measurements made by EMI, may be obtained by writing to:

Dr. F. S. Mills
Mail Stop 401A
NASA Langley Research Center
Hampton, Virginia 23665.

Table 3. Header record for plume data (format 10E10.3).

Word No.		
1	month	date
2	day	
3	year	
4	hour	start time of scan
5	minute	
6	second	
7	hour	end time of scan
8	minute	
9	second	
10	lidar site	1 = PEPCO 2 = Waverly Pt. 3 = Watson's Farm 4 = Dahlgren Beach
11	total burden	
12	minimum elevation of scan	
13	maximum elevation of scan	
14	aximuth angle of scan	
15	sea level altitude at lidar site	
16	angle	relative to north stack
17	distance	
18	rotation correction	
19	minimum Z	grid dimensions
20	maximum Z	
21	grid resolution	
22	number of points in Z direction	
23	minimum Y	
24	maximum Y	
25	number of points in Y direction	
26	file number where scan is placed on tape	
27	number of scans in grid	
28	Y centroid	
29	Z centroid	
30	centroid distance from stack	
31	Y sigma	
32	Z sigma	

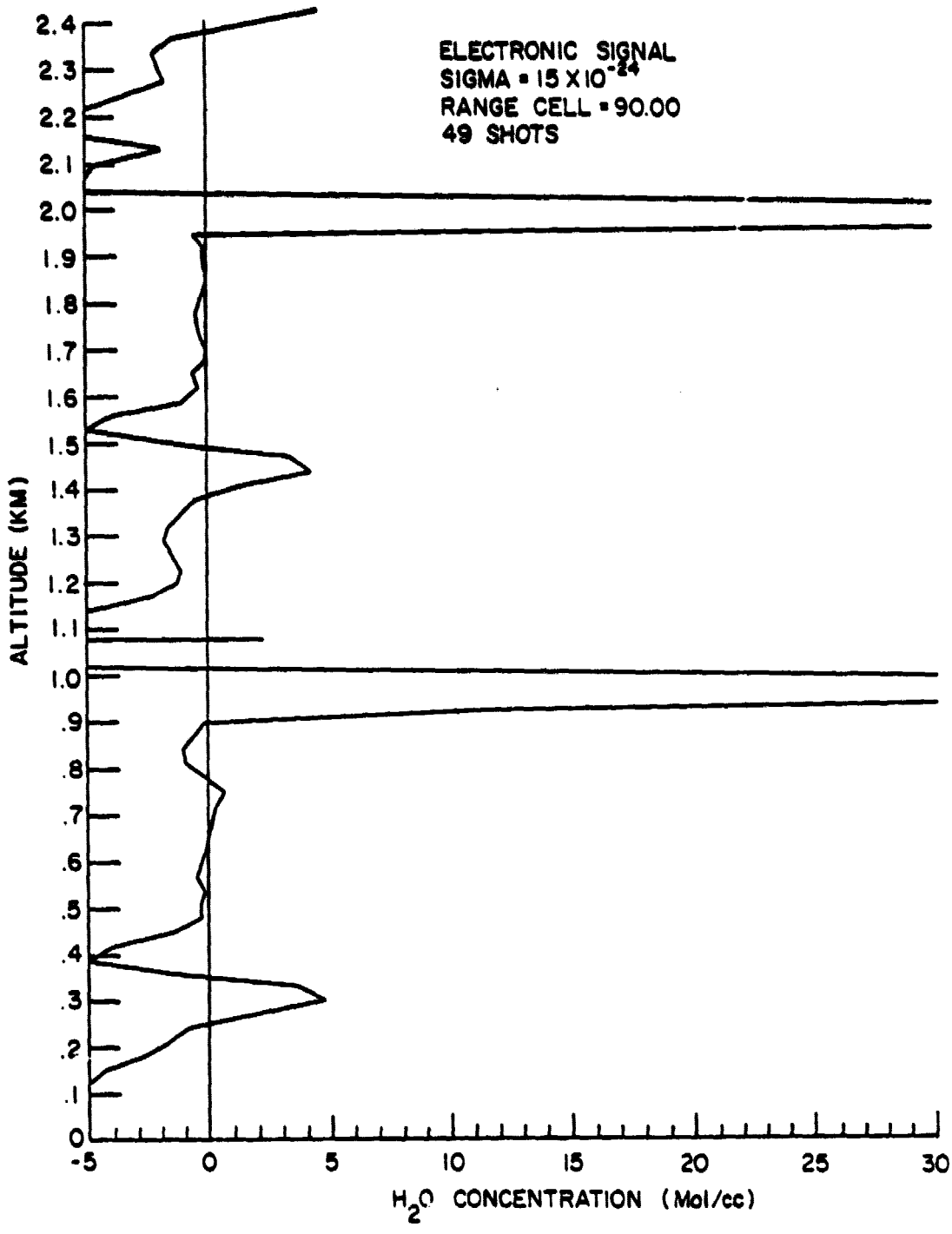

Figure 1. Calculated water vapor concentration using electronically simulated return signals.

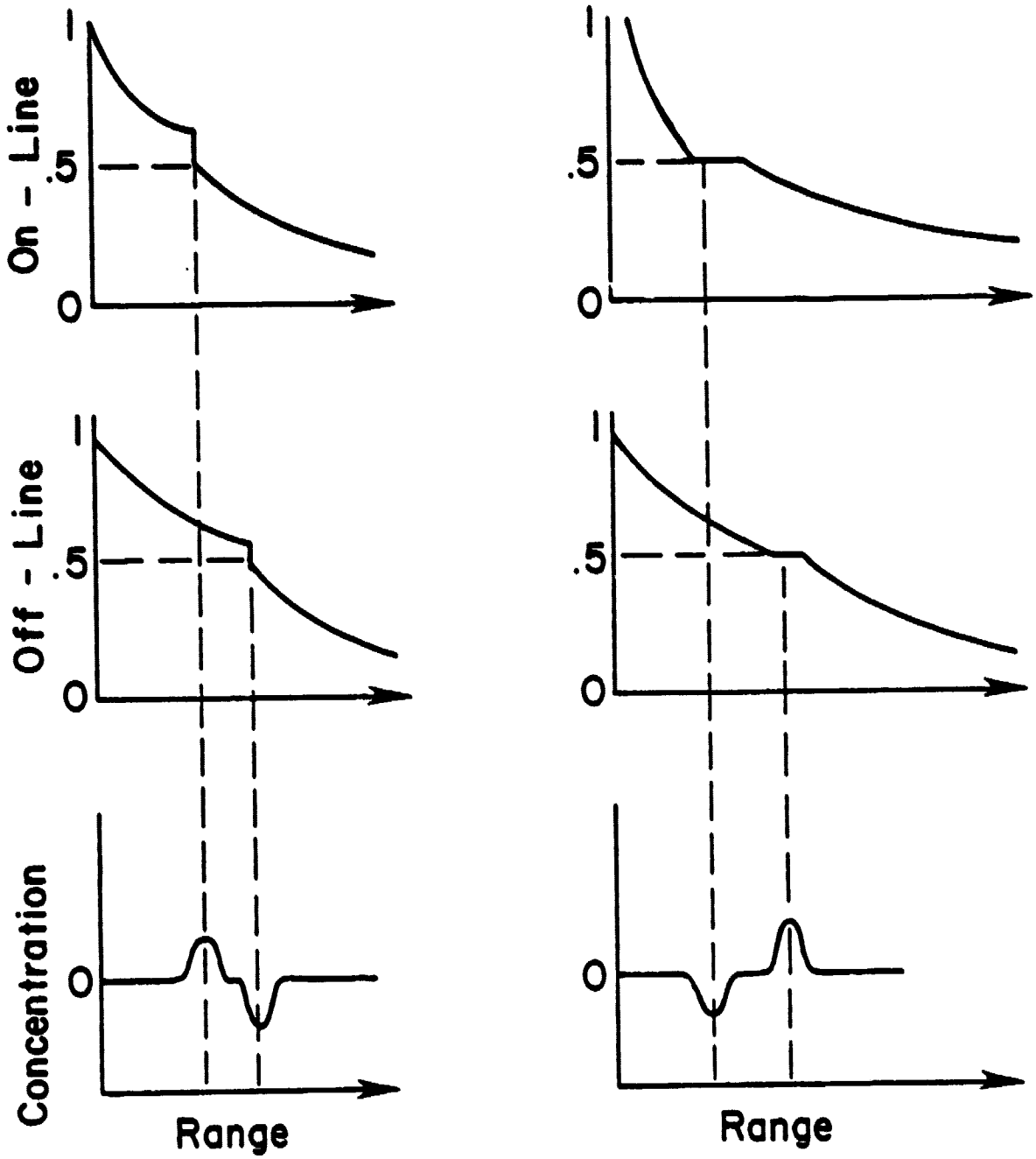

Figure 2. Effects of two types of error on calculated concentration.

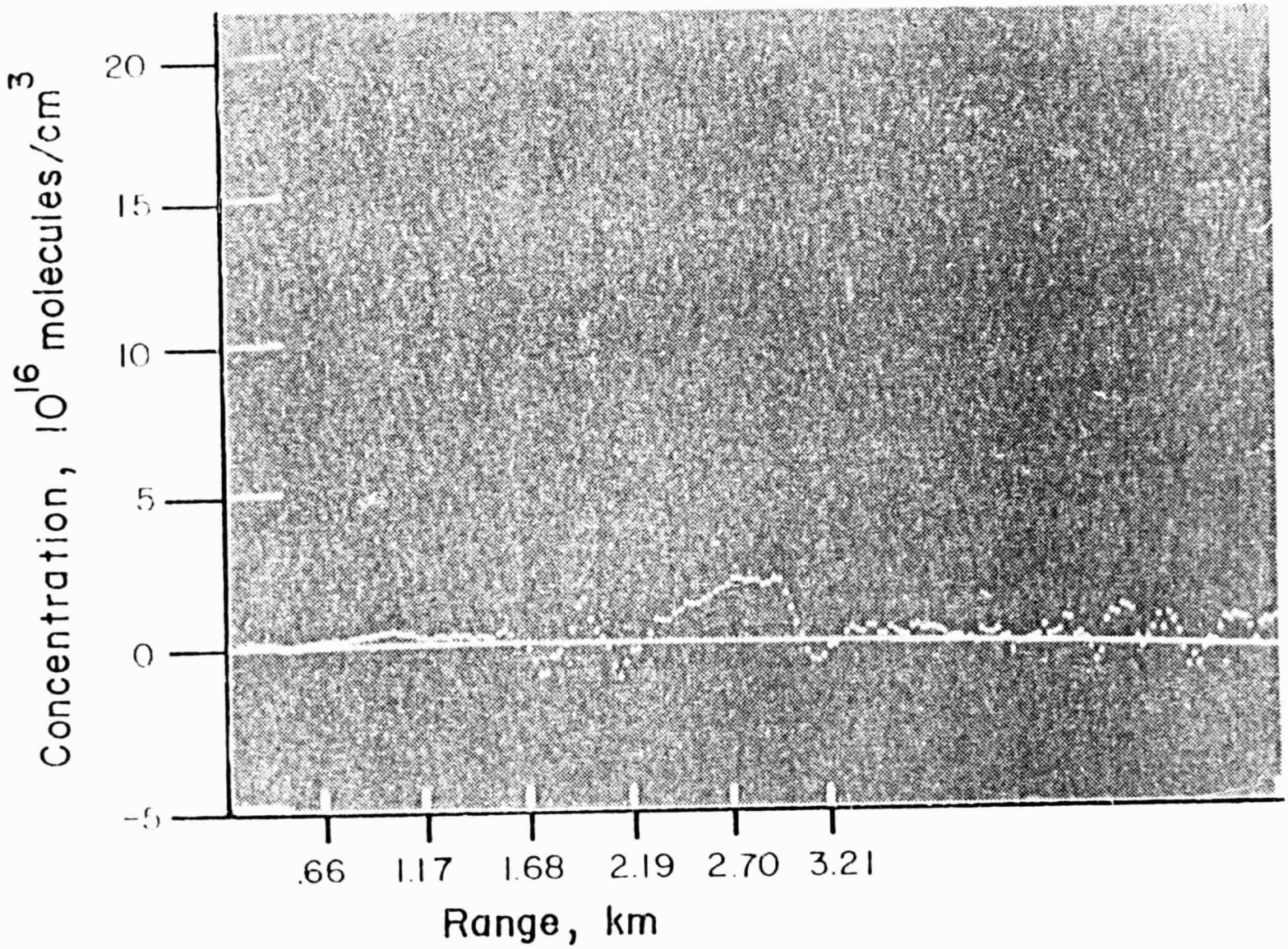

Figure 3. Attempted analytical correction of midrange problem.

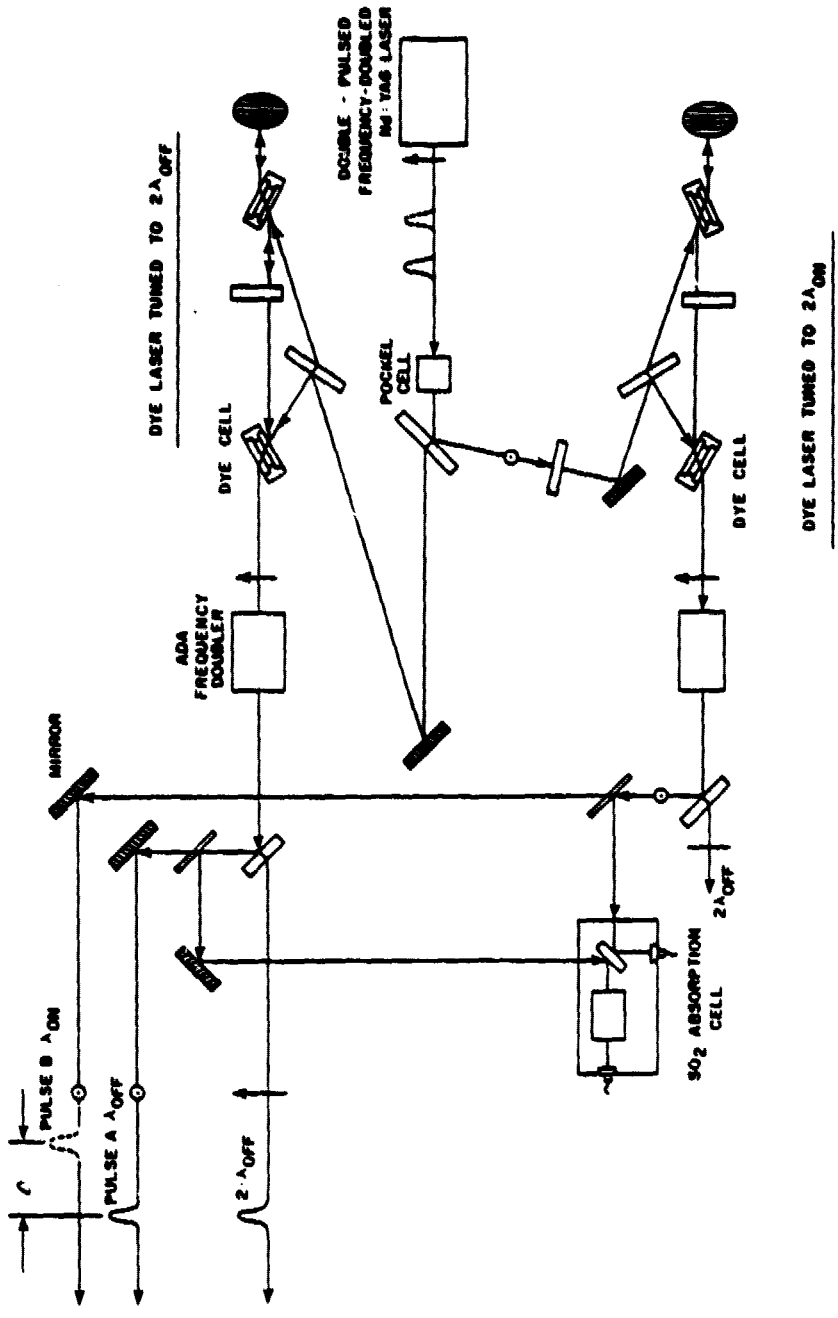

Figure 4. Double-pulse tunable UV dye laser.

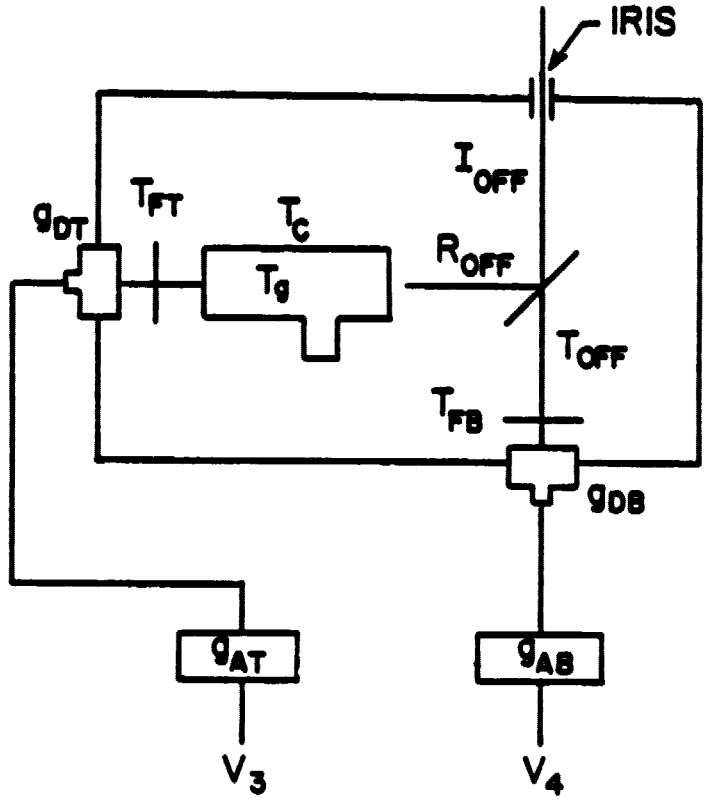

Figure 5. UV absorption cell with off-line pulse.

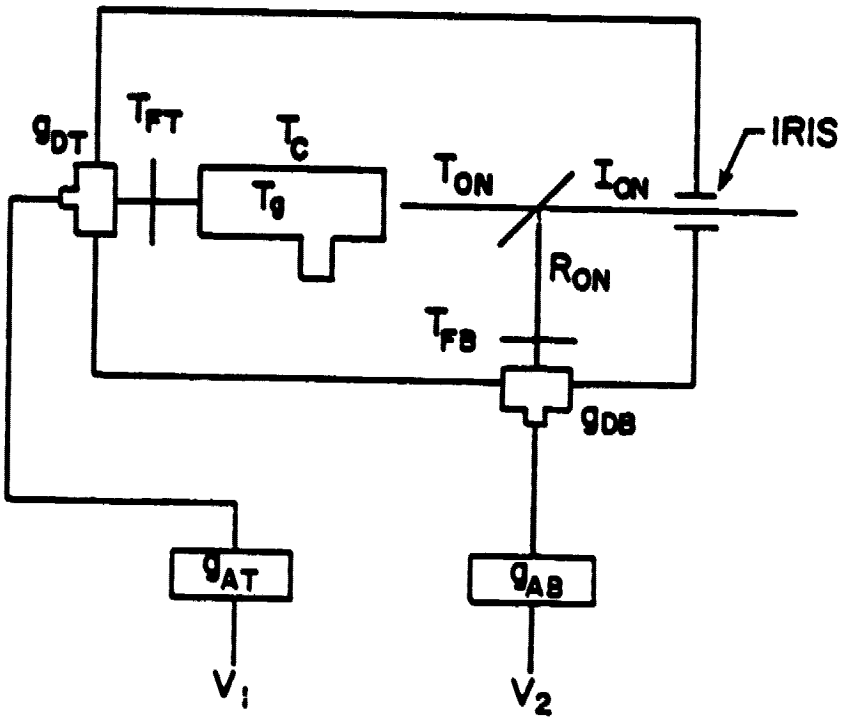

Figure 6. UV absorption cell with on-line pulse.

Figure 7. UV absorption cell.

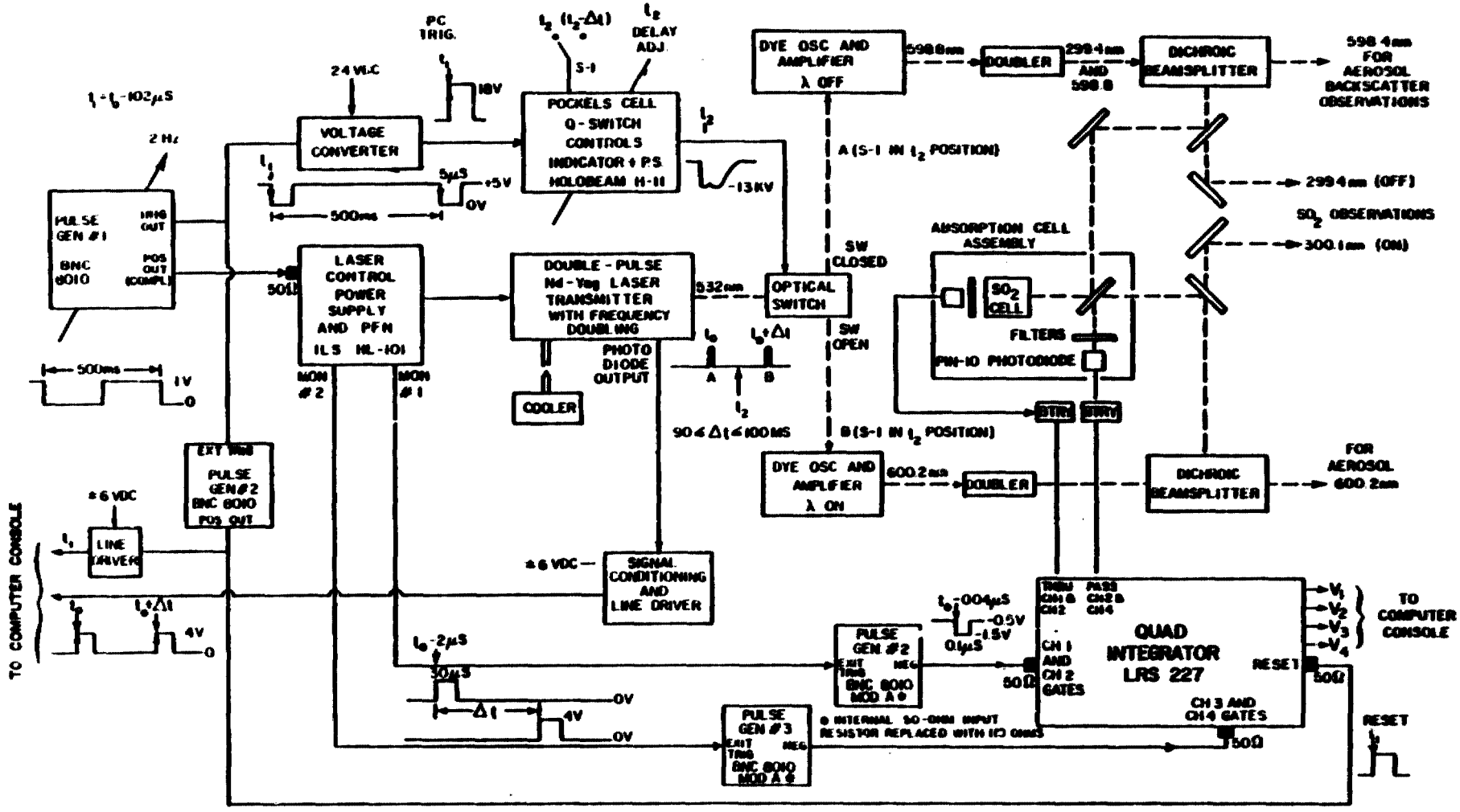

Figure 8. UV DIAL lidar timing and control using monitors 1 and 2 from ILS.

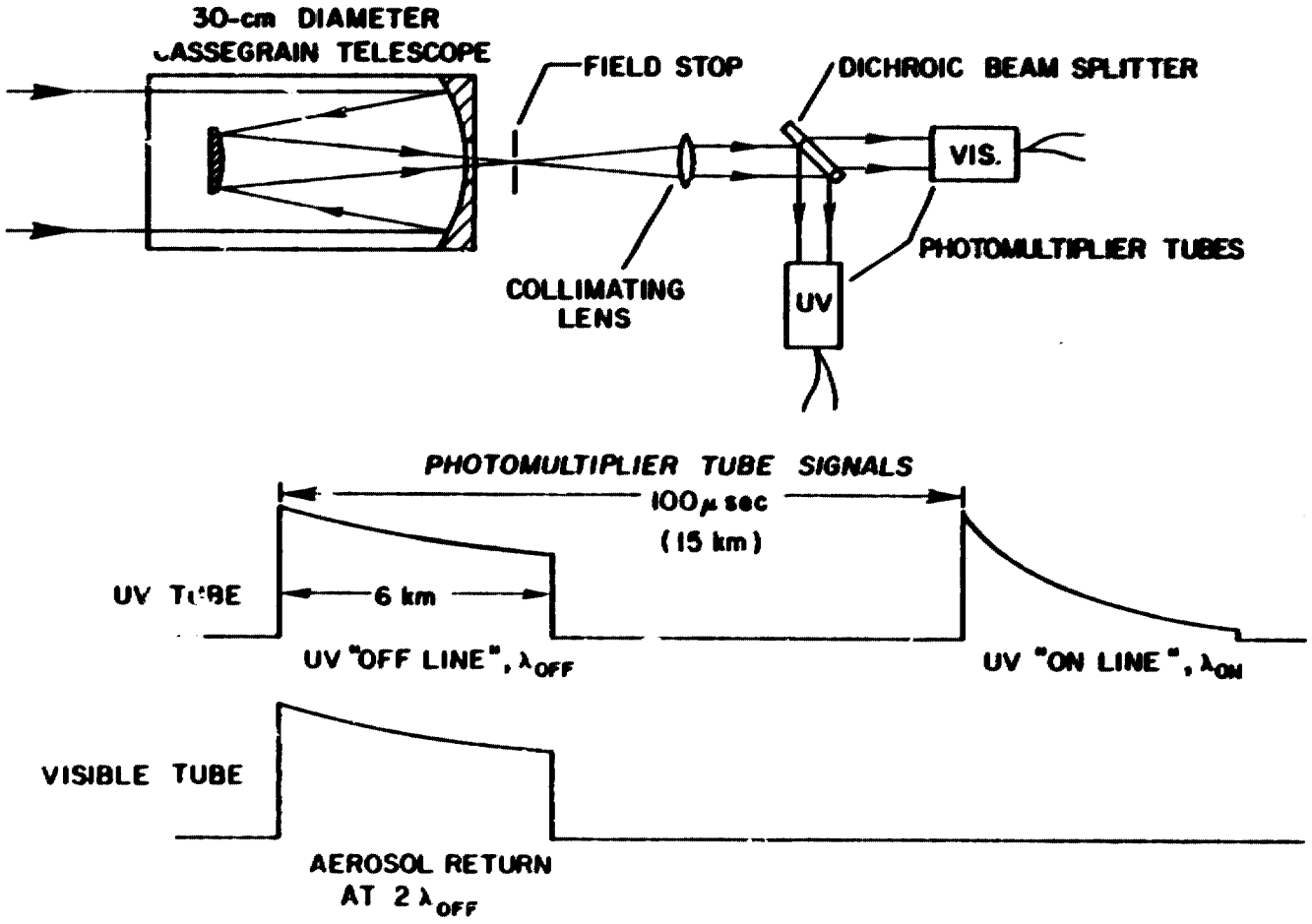

Figure 9. Block diagram of the UV DIAL receiver system.

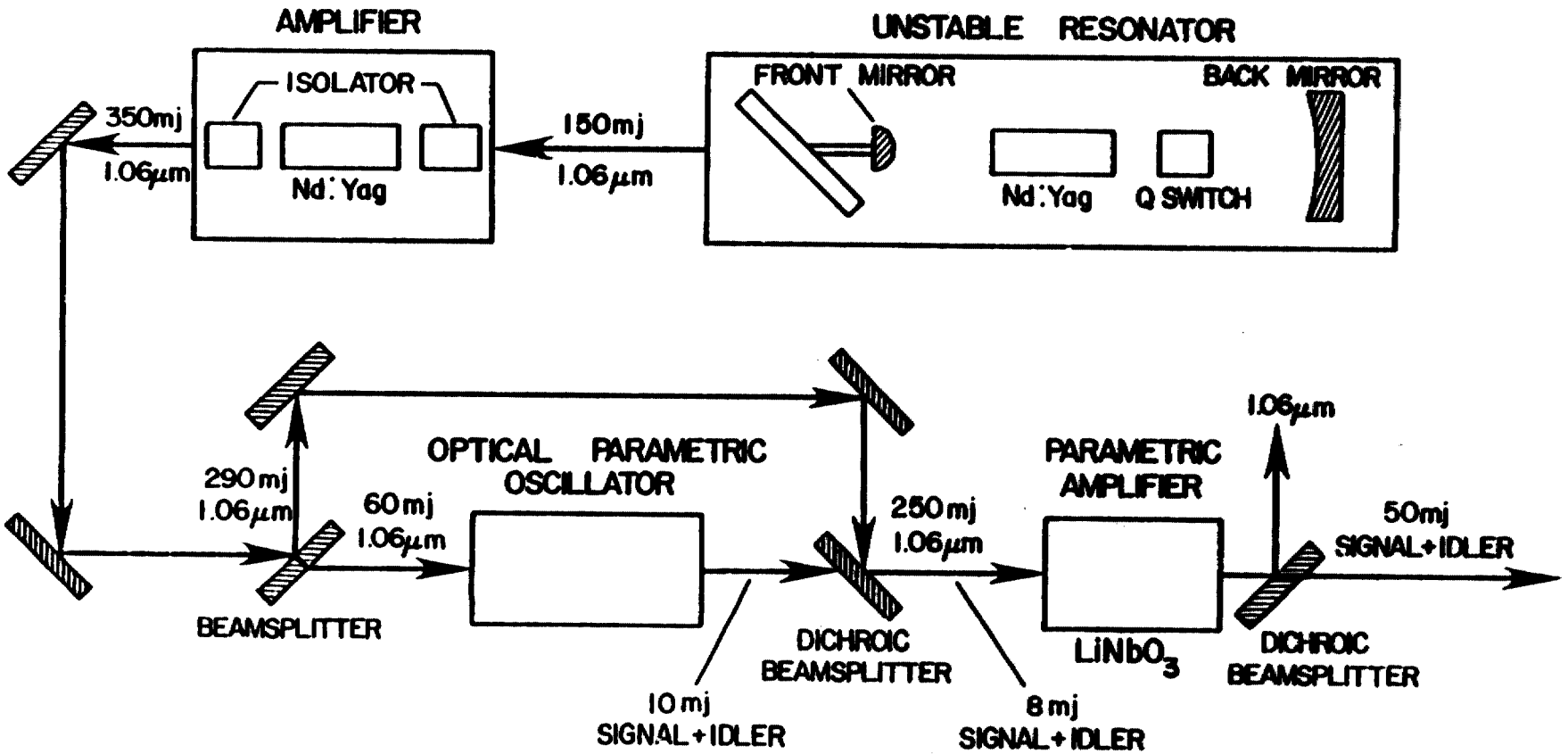

Figure 10. Block diagram of the IR tunable laser.

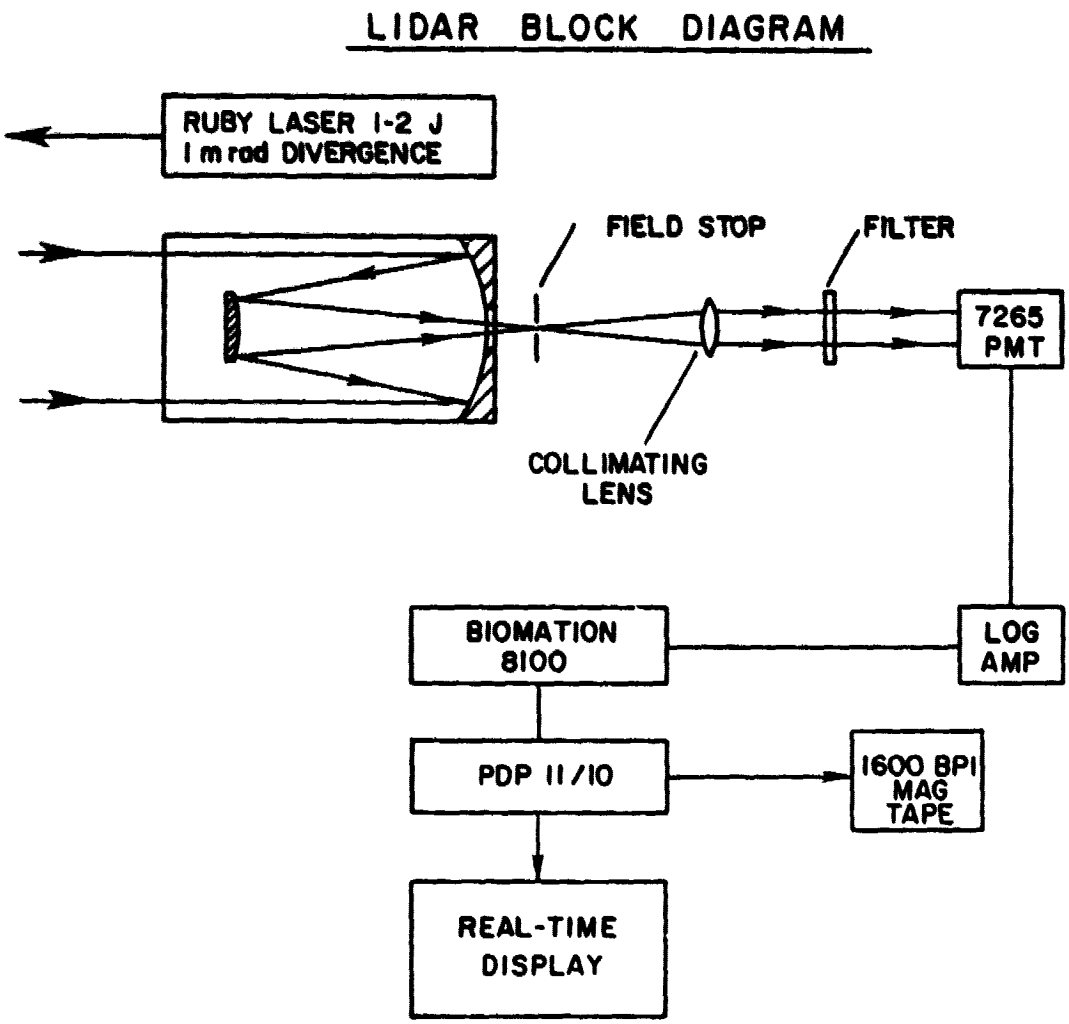

Figure 11. Block diagram of the plume dispersion lidar system.

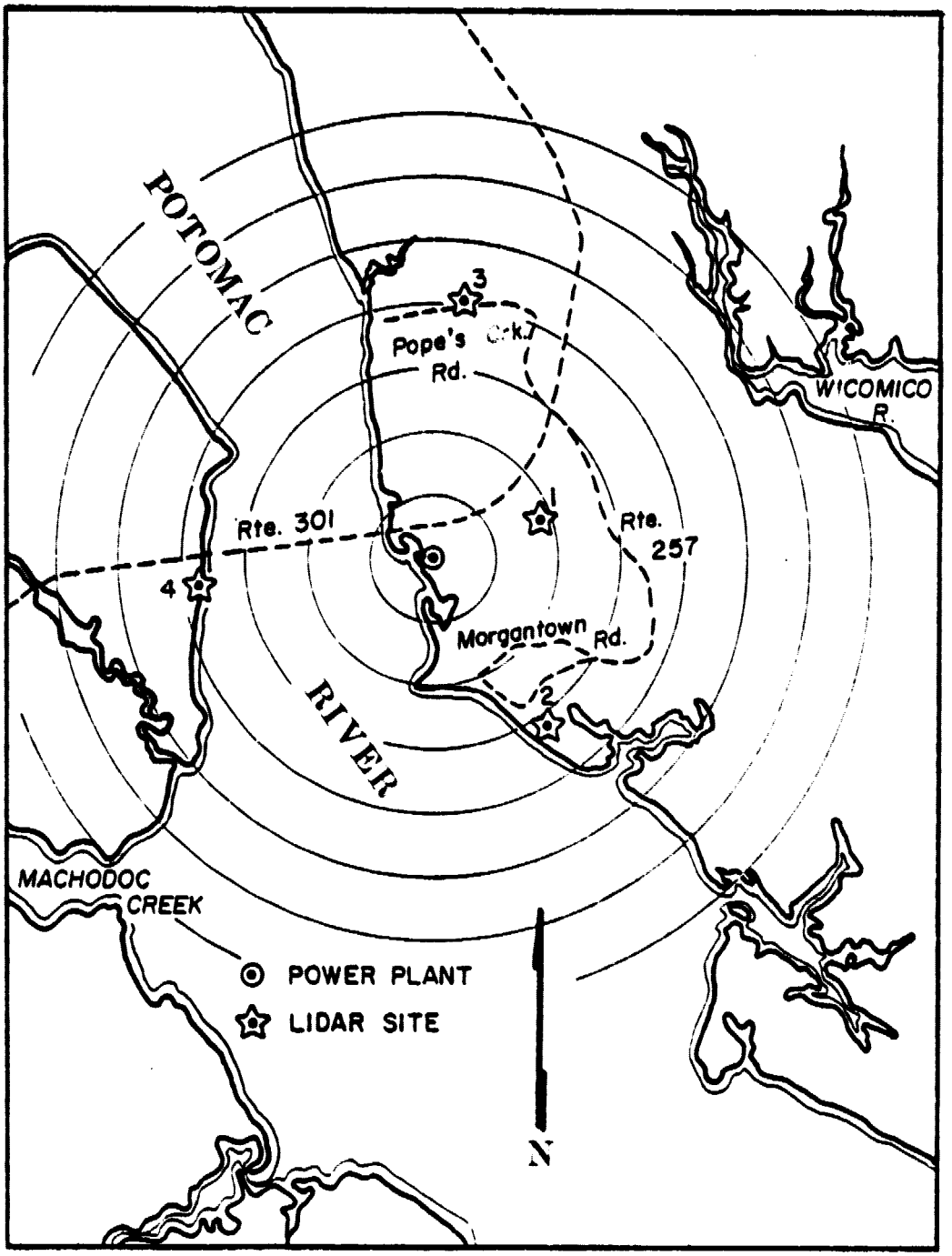

Figure 12. Map of power plant area showing lidar sites.

REFERENCES

1. Mills, F. S.; and Blais, R. N.: A Theoretical/Experimental Program to Develop Active Optical Pollution Sensors: Final Report. Old Dominion University Research Foundation Technical Report PGSTR-AP77-47.

2. Mills, F. S.; and Browell, E. V.: The Effect of Transient Digitizer Errors on DIAL Measurements. Presented at the Eighth International Laser Radar Conference, June 6-9, 1977, Drexel Univ., Philadelphia, Pa.

3. Browell, E. V.; Perillo, L.; and Mills, F. S.: Double-Pulse UV DIAL System for Measurement of SO_2. Presented at the Eighth International Laser Radar Conference, June 6-9, 1977, Drexel Univ., Philadelphia, Pa.

4. Mills, F. S.; Northam, G. B.; Hunt, W. H.; Weil, J. C.; White, C. L. Jr.; and Yelinek, F.: Validation of Plume Models for Tall Stacks Using Lidar Data. Presented at the Eighth International Laser Radar Conference, June 6-9, 1977, Drexel Univ., Philadelphia, Pa.

5. Butler, Carolyn (Jones): A Two-Dimensional Stratospheric Model of a Dispersion of Aerosol from the Fuego Volcanic Eruption. Presented at the 13th Annual Meeting of Society of Engineering Science, sponsored by JIAFF, Hampton, Va., Nov. 1-3, 1976.

6. Butler, Carolyn (Jones): A Two-Dimensional Stratospheric Model of a Dispersion of Aerosol from the Fuego Volcanic Eruption. Master's Thesis presented to faculty of the Department of Applied Sciences, College of William and Mary, Williamsburg, Va., Aug. 1977.

7. Browell, E. V.: Two-Wavelength Dye Laser. NASA Tech Brief LAR-12012, summer 1976.

8. Schotland, R. M.: Some Observations of the Vertical Profile of Water Vapor by Means of a Laser Optical Radar. Proceedings of the Fourth Symposium of Remote Sensing of Environment, Ann Arbor, Mich., April 12-14, 1966.

9. Rothe, K. W.; Brinkmann, V.; and Walther, H.: Remote Measurement of NO_2 Emission from a Chemical Factory by the Differential Absorption Technique. J. Appl. Phys., Vol. 4, No. 181, 1974.

10. Grant, W. B.; and Hake, R. D., Jr.: Calibrated Remote Measurements of SO_2 and O_3 Using Atmospheric Backscaffer. J. Appl. Phys., Vol. 36, No. 3019, 1975.

11. Hunt, W. H.: Tests of a Range-Compensated PMT Base. Presented at the Eighth International Laser Radar Conference, June 6-9, 1977, Drexel Univ., Philadelphia, Pa.

12 Herbst, R. L.; Fleming, R. N.; and Byer, R. L.: A 1.4 to 4.4 μm High Energy Angle-Tuned $LiNbO_3$ Parametric Oscillator. Appl. Phys. Lett., Vol. 25, No. 520, 1974.

13. Kibler, J. F.; and Suttles, J. T.: A Simulation of Air Pollution Model Parameter Estimation Using Data from a Ground-Based Lidar Remote Sensor. Proceedings of the AIAA 15th Aerospace Sciences Meeting, Los Angeles, Calif., January 24-26, 1977.